PERGAMON

International Journal of Heat and Mass Transfer 42 (1999) 1317–1326

International Journal of HEAT and MASS TRANSFER

Fluid flow and heat transfer in molten metal stirred by a circular inductor

Y. W. Cho[a,*], S. H. Chung[a], J. D. Shim[a], S. Dement'ev[b], S. Ivanov[c]

[a] *Metals Processing Research Laboratory, Korea Institute of Science and Technology, P.O. Box 131, Cheongryang, Seoul 130-650, Korea*

[b] *Institute of Physics, Latvian University, Salaspils-1, LV-2169, Latvia*

[c] *MHD Special Design Office, Antonias 14, Riga, LV-1248, Latvia*

Received 2 December 1997; in final form 26 June 1998

Abstract

A special electromagnetic stirrer which can produce local pulsating flows as well as an overall vortex flow in molten metals has been devised and experimentally tested using a simplified model system to evaluate its flow control characteristics and mixing efficiency. The influences of frequency, current and the waveform of current on the flow structure and heat transfer in the liquid In–Ga–Sn metal pool have been investigated. It has been found that the double frequency mode resulted in more effective heat transfer process compared to the single frequency mode, even at lower total input power, without significantly incurring a decrease in the averaged flow velocity level.

Nomenclature

Al Alfven number, $\mu_0(wI)^2/4\pi^2\rho f^2 t_z^4$
Al^* characteristic Alfven number, $\mu_0(wI)^2/(\rho V_0^{*2} t_z^2)$
$\mathbf{B}$ magnetic field
$\mathbf{b}^*$ non-dimensional magnetic field, $\mathbf{B}/B_0$
B_0 externally imposed magnetic field
C_v specific heat at constant volume
$\mathbf{E}$ electric field
$\mathbf{F}$ magnetic force
f frequency of current
I inductor current
j induced current density
k effective thermal conductivity
k^* non-dimensional thermal conductivity, k/k_{mol}
k_{mol} molecular thermal conductivity
P pressure
P_0 ρV_0^2
P_0^* characteristic pressure, ρV_0^{*2}
p^* non-dimensional pressure, P/P_0
Q heat generated by heater
r radius
Re Reynolds number, $6fr_c t_z/v$
Re^* characteristic Reynolds number, $V_0^* r_c/v$
Re_m magnetic Reynolds number, $6\ \mu_0\ \sigma f r_c t_z$
Re_m^* characteristic magnetic Reynolds number, $V_0^* r_c \mu_0 \sigma$
T temperature
t time
t^* non-dimensional time, t/t_0
t_0 r_c/V_0
t_0^* characteristic time, r_c/V_0^*
t_z tooth pitch
$\mathbf{V}$ velocity of liquid
V_0 speed of travelling magnetic field, $6ft_z$
V_0^* characteristic velocity of liquid
$\mathbf{v}^*$ non-dimensional velocity, $\mathbf{V}/V_0$
w number of coil turns
z^* non-dimensional vertical coordinate
(r, θ, z) cylindrical coordinates.

Greek symbols

α phase angle
η viscosity
θ angular coordinate

* Corresponding author

0017–9310/98/$ - see front matter
PII: S0017–9310(98)00255–5

μ_0 magnetic permeability of liquid, $4\pi \times 10^{-7}$
v kinematic viscosity
ρ density of liquid
σ electrical conductivity of liquid
Φ dissipation function.
ω angular frequency of current.

Subscripts
c container
H high
h heater
L low
r radial component
z vertical component
θ angular component.

1. Introduction

It is well known that thermal convection in molten metals during casting processes has considerable effects on the solidification structures of ingots [1–5] and well-controlled forced convection often improves the soundness of cast products [6–16], such as grain refinement and reducing macro segregation and defects. However, too much turbulent flow on the free surface of molten metals may cause surface defects in continuously cast products. Therefore, it is important to control the fluid flow and heat transfer in molten metals during solidification processes. For example, ElectroMagnetic Stirring (EMS) in continuous casting of steels [17] now becomes indispensable technology which improves solidification structures, center-line shrinkage, surface quality, inclusion content, and segregation. The same underlying principles of EMS have general applicability in continuous casting of other metals and alloys including Direct Chill (DC) casting of aluminium and its alloys. Although Electro-Magnetic Casting (EMC) of aluminium [18] could produce high surface quality products, it is not very effective in improving the internal quality of alloy billets having a wide gap between the liquidus and solidus temperatures. Therefore, it would be very useful to have an electromagnetic stirrer which can generate a desirable melt flow and control heat transfer in DC casting processes, particularly for large diameter billets of 2000 and 7000 series alloys of aluminium.

In the present study, a novel electromagnetic stirrer, consists of an inductor and a special complex current generator, which can generate local pulsating flows as well as an overall vortex flow in liquid metal, has been devised and its flow control characteristics and mixing efficiency have been evaluated using the In–Ga–Sn model liquid metal system. In addition, the flow velocity in the molten aluminium pool for given electromagnetic and geometric conditions could be estimated by adopting a non-dimensional analysis method and the experimental. From these results, an optimized EM stirrer design and control parameters could be proposed for applications to DC casting processes of large diameter aluminium alloy billets.

2. Design of EM stirrer

2.1. Single pole inductor

A schematic drawing of the inductor designed in the present study is shown in Fig. 1(a). It is basically a short linear cylindrical inductor with a single pole, which is suitable for applications where the height of the inductor is restricted as in DC casting processes. Unlike other common inductors, it has a single pole structure which produces a travelling magnetic filed along the axial (vertical) direction. Ring-shaped currents are induced in a liquid-metal pool placed inside the inductor and the induced currents interact with the applied magnetic field and its interaction produces the electromagnetic volume forces. The principle is exactly the same as that of a conventional 3-phase induction motor, except that the magnetic field is not rotating but travels linearly in the present inductor. The inductor was designed so that the electromagnetic force density has a maximum value on the inductor interior surface at 60 Hz and decreases toward the center. The decrease of the electromagnetic forces along the radial direction toward the center produces forced convection flows in the liquid metal pool.

The inductor designed and used in the present study has 16 yokes made of 0.5 mm thick silicon steel sheets and each yoke has 4 teeth and three slots for 3 coils. The inside diameter and height of the inductor are 150 and 133.2 mm, respectively. The tooth pitch t_z is 33.3 mm and each coil has 160 turns of 1.5×5 mm rectangular copper wire electrically insulated with high temperature enamel. The inductor has a delta connection and the maximum allowable current without additional cooling is about 20 A for each phase. A typical time averaged magnetic flux density distribution inside the inductor is given in Fig. 1(b).

2.2. Complex current generator

A special complex current generator which can produce any arbitrary waveform of 3-phase current including multifrequency modes and periodic reversal of the direction of a travelling magnetic field has been made to control the inductor and Fig. 2 shows its simplified circuit diagram as well as a typical waveform generated. It consists of a 3-phase voltage regulator, personal computer, and a modified inverter. A variable transformer regulates the input voltage of the inverter in order to control the input current to the inductor. Using a PC program based on the pulse width modulation method, any arbitrary

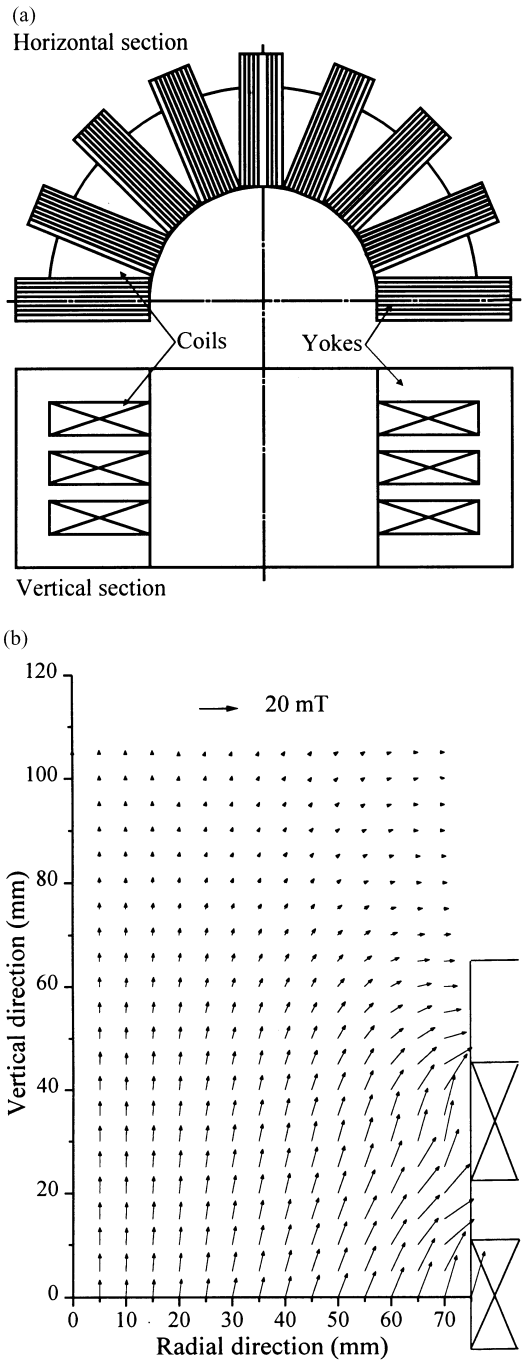

Fig. 1. (a) Schematic drawing of inductor and (b) distribution of B.

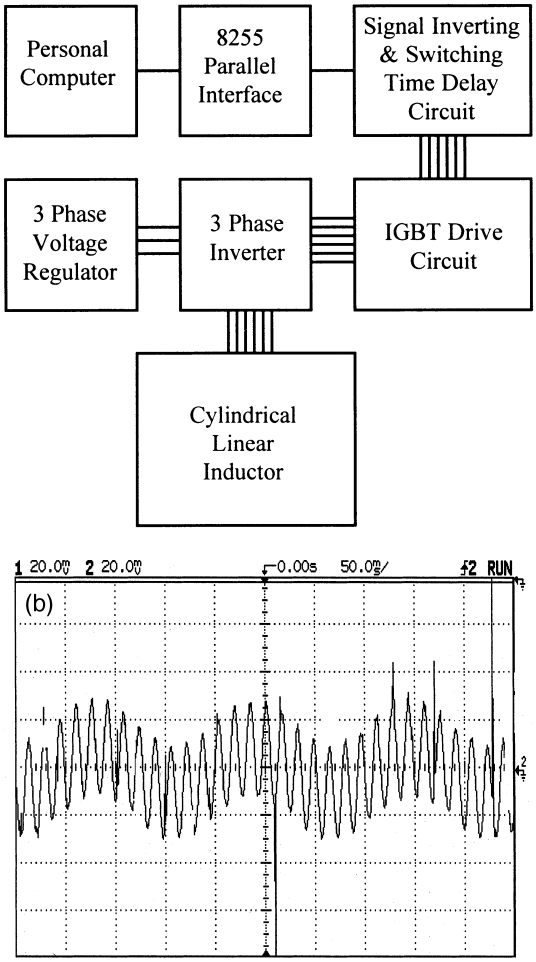

Fig. 2. (a) Circuit diagram of complex current generator and (b) waveform for 6+60 Hz.

waveform can be generated and it is converted into the electronic signals by an 8255 based parallel interface and a signal inverting and switching time delay circuit. These signals now drive six IGBTs in the inverter to feed the inductor with the same waveform of current as the one generated by the PC program. The frequency range of the complex current generator used in the present study is from DC up to 1 kHz and the maximum voltage and current are 220 V and 32 A, respectively. The basic principle of multifrequency stirring is explained in detail by Spitzer et al. [19] who used a similar current source for rotational stirring of mercury in a cylindrical container.

3. Experimental

3.1. Experimental setup

As the shape of the sump in DC casting processes is rather complicated depending on the casting conditions, a simplified physical model has been adopted as sche-

matically drawn in Fig. 3. A brass container (1), having a spherically contoured bottom partially filled with the In–Ga–Sn eutectic alloy (2) which has a melting point of about 284 K, was used for modeling both the DC casting mold and solidified shell. The brass container is placed inside a water jacket (3) to keep the temperature of the container within ± 0.1 K by regulating the flow rate and temperature of cooling water (4). At the center of the melt free surface, a heater (5) made of a copper tube and heating wire is installed and the input power of the heater was regulated by a DC power supply. The outside surface of the heater and the inside surface of the brass container are pre-coated with tin in order to maintain a good thermal contact between these surfaces and the liquid eutectic alloy. The top of the container is thermally insulated and a three dimensional transverse unit (6) is mounted on a container cover plate (7) to manipulate either velocity or thermocouple probes (8). The whole system is located inside the inductor (9) as shown in Fig. 3.

3.2. Experimental procedure

The flow structure on the free surface was investigated by visual observation with the streak photography. Two different shapes of velocity probes [20, 21] made of 3 mm diameter and 5 mm long NdFeB magnets were used to measure the vertical and radial components of velocity in the liquid metal. The signals from the velocity probes were collected by a high impedance digital potentiometer controlled by a personal computer. A low pass filter was used to reduce the noise which originates from the induced current in the liquid metal by the externally applied travelling magnetic field. In addition, a preliminary experiment was made to evaluate the relative magnitude of noise to the real hydrodynamic signal. In the middle of the measurement, the inductor current was switched off and the change of the signal level was monitored. The signal level gradually decreased by not more than about 3% of the previous level. Therefore, it is believed that the velocity probe used in the present study could measure the time averaged velocity with reasonable accuracy.

The temperature distributions in the liquid metal pool were also measured with a temperature probe of an 0.08 mmϕ k-type thermocouple. The temperatures of the heater and container were also measured by thermocouples located about 1 mm below the surfaces of the heater and container as shown in Fig. 3. All of the thermocouples were connected to another digital potentiometer equipped with a multichannel scanner, which is controlled by the personal computer. At the same time, the voltage and current of the heater as well as the inductor current were controlled and recorded.

3.3. Evaluation of effective thermal conductivity

The simple analysis of the heat transfer process in the physical model system used in the present study, as schematically drawn in Fig. 4, can be started from the equation of energy [22];

$$\rho C_{\mathrm{v}}\left[\frac{\partial T}{\partial t}+(\mathbf{V}\nabla)T\right]=k_{\mathrm{mol}}\nabla^2 T+\eta\Phi+\sigma(\mathbf{E}+\mathbf{V}\times\mathbf{B})^2. \quad (1)$$

The last term on the RHS of the equation is a Joule heating effect due to the eddy currents induced by externally applied magnetic fields. The first term on the LHS and the third and last terms on the RHS of the equation are considered to be negligible for the following reasons. In the present study, only the steady-state condition is considered and the viscous dissipation term is negligible due to the relatively small value of Φ in our system. In

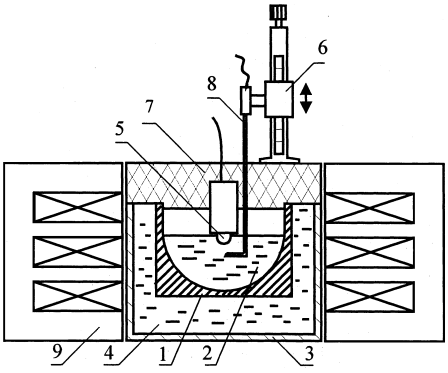

Fig. 3. Schematic drawing of experimental setup: (1) brass container, (2) In–Ga–Sn eutectic alloy, (3) water jacket, (4) cooling water, (5) heater, (6) three-dimensional transverse unit, (7) container cover plate, (8) velocity or thermocouple probes, and (9) inductor.

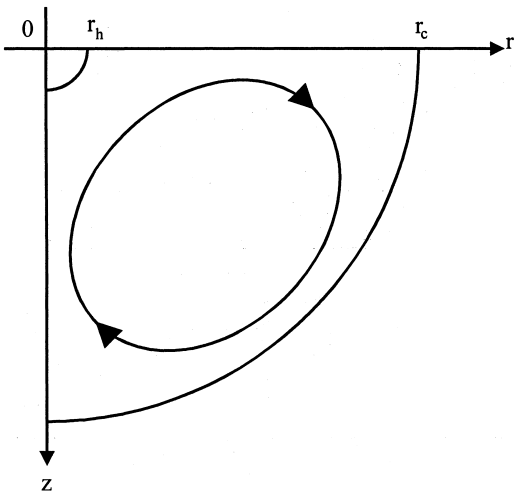

Fig. 4. Schematic drawing of physical model.

addition, it was confirmed by a preliminary experiment that the temperature of the liquid metal did not rise more than 0.2 K without water cooling for at least 3 min under the range of electromagnetic fields adopted in the present study, while the average temperature difference between the heater and liquid metal container for the same period of time was about 4.5 K. This result directly indicates that the influence of the Joule heating on the melt temperature was not significant under the conditions adopted in our experiment. Therefore, the heat transfer in the liquid metal can be determined on the whole by two heat transfer mechanisms; conduction by the molecular diffusion and convection, both natural and forced ones, by the flow in the liquid metal.

If we solve the Fourier equation for a half-spherical system with an adiabatic free surface and a heat source at the center of the sphere, the following solution will be obtained for a solid body in a steady state condition:

$$Q = 2\pi k_{\mathrm{mol}}(T_{\mathrm{h}} - T_{\mathrm{c}})/(r_{\mathrm{h}}^{-1} - r_{\mathrm{c}}^{-1}). \tag{2}$$

As a first approximation, a similar type of solution can be adopted to estimate the volume averaged effective thermal conductivity of the liquid metal pool;

$$k = \frac{Q(r_{\mathrm{h}}^{-1} - r_{\mathrm{c}}^{-1})}{2\pi(T_{\mathrm{h}} - T_{\mathrm{c}})} \tag{3}$$

where k is defined as;

$$k = k^* \cdot k_{\mathrm{mol}} \tag{4}$$

Here, k^* is a non-dimensional coefficient and $(k^* - 1)$ indicates the degree of the increase in thermal conductivity of the liquid metal pool due to the convective heat transfer including both natural and forced convection terms. If there is no movement in the liquid metal including natural convection, k^* will be equal to 1. Therefore, the heat transfer as well as the flow behavior in the liquid metal pool induced by externally applied electromagnetic fields can be characterized with the use of k^* values obtained from the local temperature measurements.

4. Results

4.1. Single frequency mode

The radial and vertical components of local flow velocity in the liquid metal pool were measured at 60 Hz for the downward direction of travelling magnetic field to envisage the flow structure and the results are shown in Fig. 5. The V_z increased along the depth of the pool and after reaching a maximum value it decreased. It also increased with an increase in current. However, the depth where the maximum V_z occurred did not change as the inductor current increased. This result indicates indirectly that the general flow structure did not change with current. The maximum local velocity of about 9 cm s^{-1} was obtained at 7 A and it is linearly proportional to the inductor current as clearly indicated in Fig. 6. This result agrees very well with that of numerical calculation [23] shown as the solid line in Fig. 6. From these results and those of numerical calculation [23], it seems that a flow structure having a simple toroidal vortex is formed in the liquid metal pool, as schematically shown in Fig. 4 when a single frequency mode is used. Near the container wall, the fluid flows downward and upward near the center of the pool when the direction of the travelling magnetic field is downward. It seems that rather small stagnant zones exist at the bottom of the melt pool as well as just below the heater. The upward travelling magnetic field led to a similar flow structure but with the opposite direction of the vortex flow. However, it was observed that the stagnant zone becomes slightly larger with the upward travelling magnetic field, although the velocity level did not change significantly as given in Fig. 5(b). Depending on the current level, two different types of flow pattern were observed in our model system. When the current was below about 3 A, several relatively large scale eddies of about 10 to 15 mm were observed and the local fluctuation of temperature due to those eddies were detected as indicated in Fig. 7(a). As the current increased, an overall toroidal vortex flow started to develop and its size increased with current. Once the toroidal vortex flow fully developed, the flow structure did not change with current and the local fluctuations of temperature could not be detected as shown in Figs 7(b) and (c). In this regime, further increase in current level would have increased only the magnitude of the local flow velocity but did not change the flow structure.

The distributions of temperature fields along the vertical direction at the center of the liquid metal pool for different current levels are given in Fig. 7. Near the heater surface ($z = 6$ to 15 mm), a sharp temperature gradient was observed but the temperature variation in the bulk ($z > 15$ mm) was rather small. The temperature gradient near the container wall ($z = 35$ to 45 mm) was very small because the heat flux density here is significantly smaller than that near the heater since both the heater and container have hemispherical geometry. The perturbation of temperature in the bulk was observed when the current level is low (1 to 3 A) as clearly seen in Fig. 7(a). As explained before, it seems that the temperature perturbation is connected to the relatively large scale eddies observed in the transition mode of flow. The dependence of the boundary layer thickness, which is defined as a distance from the heater to the point where T is equal to

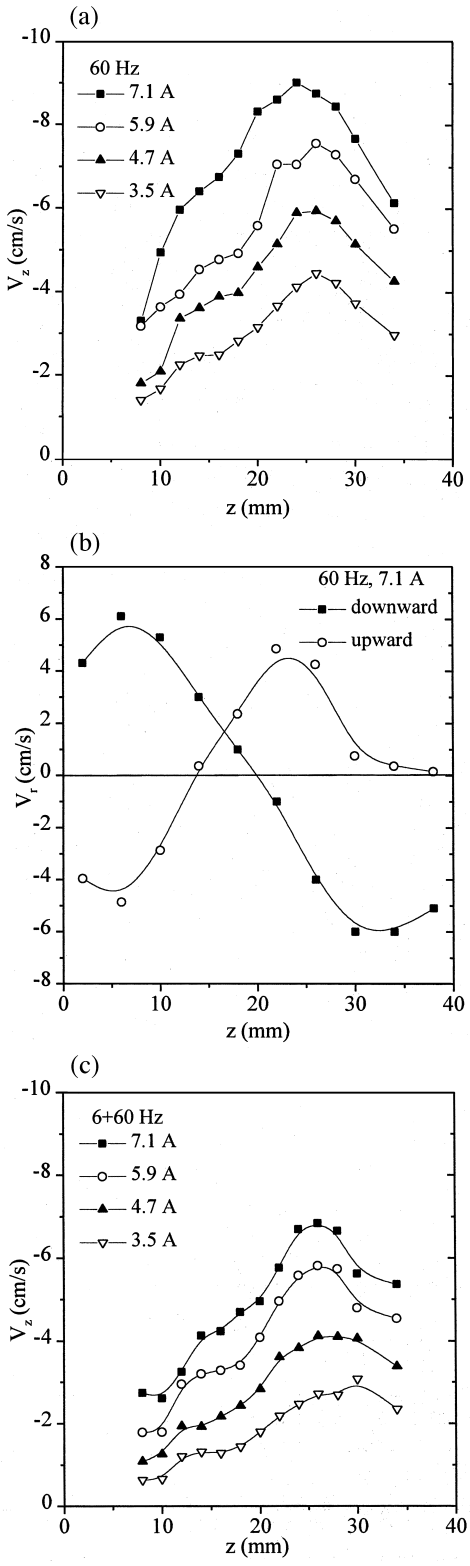

Fig. 5. Velocity distributions at 60 Hz along (a) at $r = 0$, (b) at $r = 12$, and (c) at 6+60 Hz and at $r = 0$.

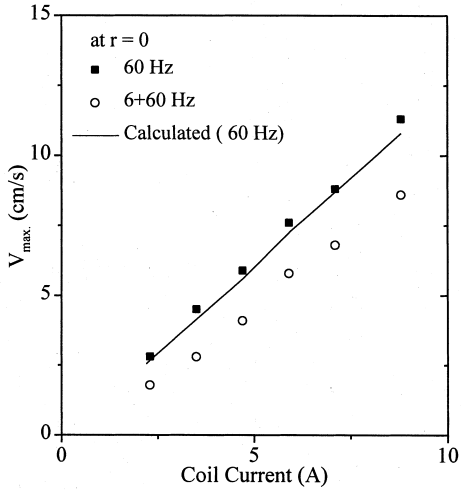

Fig. 6. Effect of coil current on V_z.

$T_h - 0.9(T_h - T_c)$, on the current level along the vertical axis is presented in Fig. 8. Up to about 3 A below which the transition mode flow structure is prevailing, the boundary layer thickness sharply decreased with current, but above 3 A it hardly depended on the current level.

The values of k^* were obtained from the measured temperature data at different current and frequency levels and the results are given in Figs 9 and 10. The inductor used in the present study was designed to produce maximum electromagnetic force in the liquid metal at 60 Hz and the result that the value of k^* has a highly expressed maximum between 55 and 65 Hz as clearly seen in Fig. 9 confirms the credibility of our inductor design technique. It has also been found that the relationship between k^* and current is linear as shown in Fig. 10. For example, k is estimated, using the empirical formula shown in the figure, to be about 4.3 times k_{mol} at 15 A.

When the direction of the flow near the container wall is upward rather than downward, k^* decreased but only by about 5% compared to the downward flow case. In addition, a periodic change in the direction of the travelling magnetic field with between 1 and 5 s time constant, resulted in the reduction of k^* by approximately 10–20%. It seems that the inertial force damped the stirring intensity when the direction of the flow is reversed relatively fast.

4.2. Multifrequency mode

An almost identical series of experiments as those with the single frequency mode were carried out with multifrequency mode. When the directions of low (6 Hz) and high frequency (60 Hz) travelling magnetic fields are the same, it appeared that the overall vortex flow pattern did not change. However, the time averaged velocity decreased to about 7 cm s^{-1} from about 9 cm s^{-1}

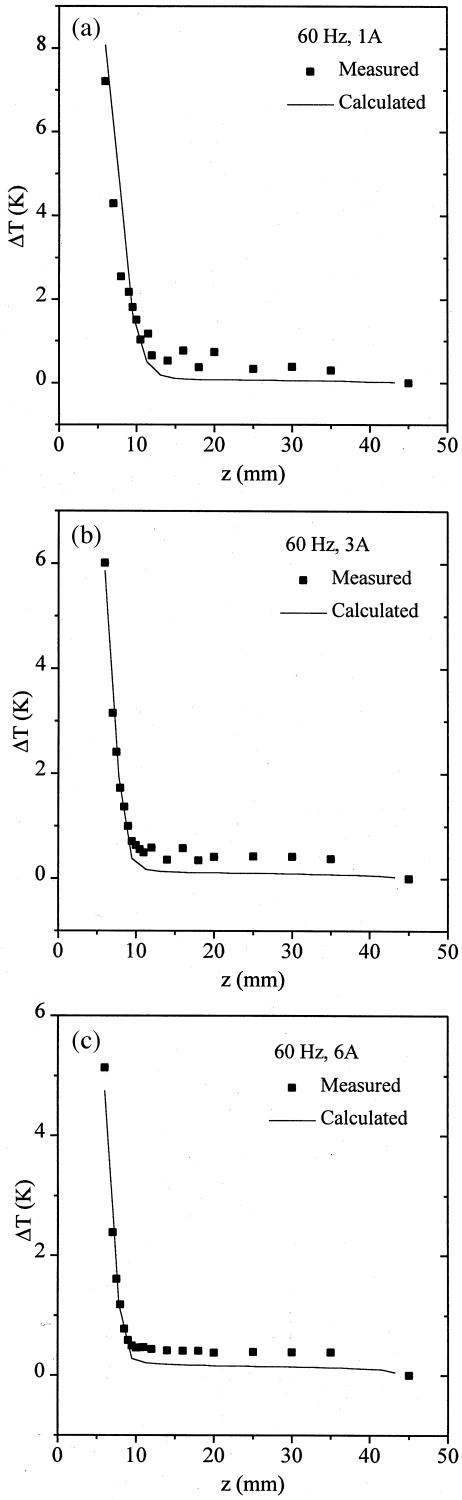

Fig. 7. Temperature distribution along z direction; at (a) 1 A, (b) 3 A, and (c) 6 A coil current.

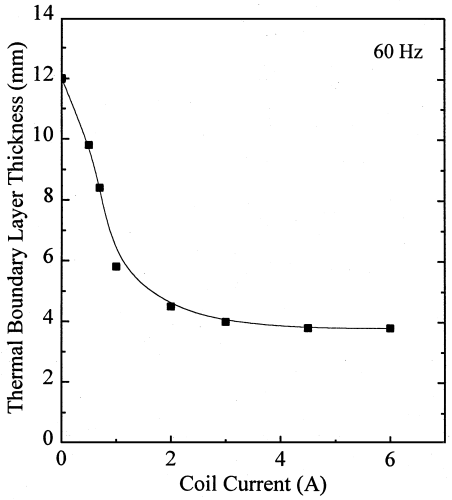

Fig. 8. Effect of coil current on thermal boundary layer thickness.

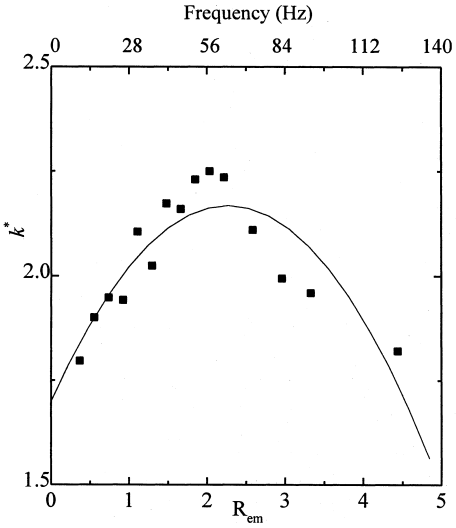

Fig. 9. Dependence of k^* on magnetic Reynolds number at 4 A coil current.

measured with the single frequency mode. Although the reactive power to the inductor with the multi-frequency mode was only about 55% of the single frequency mode, data for both was obtained at the same nominal current level of 7 A. As shown in Fig. 6, a linear relationship between the velocity and current is also preserved with the multi-frequency mode. In the meantime, the result of temperature measurements clearly shows that the decrease in the time averaged velocity did not necessarily lead to a corresponding reduction in the effective thermal conductivity of the liquid metal pool as shown in Fig. 10. On the contrary, the increase in k^* up to about 20% of the value, obtained with the single frequency mode, could

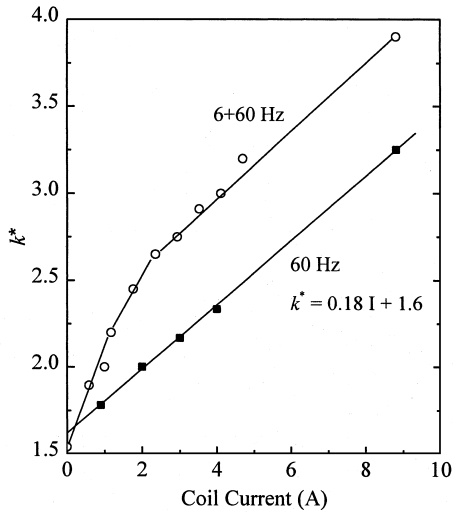

Fig. 10. Influence of current on k^*.

be predicted at the nominal current of 15 A based on the empirical formula shown in Fig. 10.

The linearity between k^* and current was not strictly maintained with the multi-frequency mode as indicated in Fig. 10. This result again seems to be related to the transition of the flow structure. When the direction of the high frequency current is opposite to that of the low frequency current, neither the effective thermal conductivity nor the velocity changed significantly compared to the results with the single frequency mode.

5. Discussions

5.1. Non-dimensional analysis

The fluid flow driven by externally applied electromagnetic fields in an electrically conducting liquid is governed by the following equations:

$$\frac{\partial \mathbf{v}^*}{\partial t^*} + (\mathbf{v}^*\nabla)\mathbf{v}^* = -\nabla p^* + \frac{1}{Re}\nabla^2\mathbf{v}^* + Al(\nabla \times \mathbf{b}^*) \times \mathbf{b}^* \quad (5)$$

$$\operatorname{div} \mathbf{v}^* = 0 \quad (6)$$

$$\frac{\partial \mathbf{b}^*}{\partial t^*} = \nabla \times (\mathbf{v}^* \times \mathbf{b}^*) + \frac{1}{Re_m}\nabla^2\mathbf{b}^* \quad (7)$$

$$\operatorname{div} \mathbf{b}^* = 0 \quad (8)$$

which are derived by adopting the following variables;

$$V_0 = 6ft_z \quad (9)$$

$$B_0 = \frac{\sqrt{2}\mu_0 wI}{t_z} \quad (10)$$

$$t_0 = r_c/V_0 \quad (11)$$

$$P_0 = \rho V_0^2 = \rho(6ft_z)^2. \quad (12)$$

From the equations (5) and (7), the following non-dimensional numbers can be defined.

$$Re = \frac{6ft_z r_c}{v} \quad (13)$$

$$Al = \frac{\mu_0}{4\pi^2\rho}\frac{(wI)^2}{f^2 t_z^4} \quad (14)$$

$$Re_m = 6\mu_0 \sigma f r_c t_z \quad (15)$$

The typical ranges of these non-dimensional numbers calculated for the physical model system and for an example of the real DC casting processes agree reasonably well with each other as shown in Table 1. It means that the experimental data obtained from the physical model system in the present study can be reliably applied to estimate the velocity level as well as the overall flow structure in an aluminum melt pool, if only the differences in the electrical boundary and geometry conditions between the two are not too significant. For example, the time averaged velocity distribution along the melt pool axis, as a first approximation, can be calculated using the empirical formulae (16) and (17) obtained from Fig. 5(c) by adopting the non-dimensional variable v_{z^*} and z^* as given in equations (18) and (19) described below.

$$v_{z^*} = -0.78z^{*2} + 0.84z^* - 0.06 \quad \text{for 60 Hz} \quad (16)$$

$$= -0.6z^{*2} + 0.7z^* - 0.08 \quad \text{for 60 and 6 Hz} \quad (17)$$

$$v_{z^*} = V_z/(V_0 Al^{1/2}) = V_z t_z/(\mu_0/\rho)^{1/2} wI \quad (18)$$

Table 1
Comparison of non-dimensional numbers between model and DC casting condition

Non-dimensional numbers	Model (r_c = 45 mm, 1–15 A, 6–60 Hz)	Aluminium DC casting (r_c = 120 mm, 1–50 A, 6–60 Hz)
Re^*	$1\times10^3-3\times10^4$	$1\times10^4-2\times10^5$
Al^*	$2.4\times10^{-3}-0.14$	$3.3\times10^{-3}-0.26$
Re_m^*	$1\times10^{-3}-4\times10^{-2}$	$7\times10^{-3}-1.5\times10^{-2}$

$$z^* = z/r_c \tag{19}$$

If we consider the conditions for the DC casting process of aluminium represented in Table 1, it is expected to have V_z maximum of about 20 cm s^{-1} at 50 A.

The result of analysis on the effective thermal conductivity data obtained from the experiment with the simplified physical model adopted in the present study does not allow us to predict k^* in the molten aluminium pool of real DC casting processes because the main part of the heat resistance is concentrated at the boundary layer near the heater in the model liquid metal system unlike in the real processes. However, the dependence of k^* on the frequency ($I = 4$ A) can be generalized using the following empirical formula approximated from the experimental data shown in Fig. 9.

$$k^* = -0.1Re_m^2 + 0.4Re_m + 1.7 \tag{20}$$

Using this formula, it is possible to calculate the optimum frequency for a given aluminium melt based on the effective thermal conductivity point of view. For example, the optimum frequency is estimated to be about 10 Hz for the same conditions as given in Table 1. The optimum frequency of the inductor suitable for the aluminium melt is estimated between 5 and 10 Hz based on the numerical analysis [23] of electromagnetic force and flow velocity distributions in the melt. These results indicate that it is possible to design and select optimum ranges of control parameters, such as frequency and current, of the inductor suitable for a given DC casting process utilizing the non-dimensional analysis with the results of the physical model experiment.

5.2. Multifrequency mode

When high and low frequency currents are fed to an inductor simultaneously, the electromagnetic force components generated in a molten metal pool located inside the inductor can be calculated using the following equations.

$$F_r = j_\theta \cdot B_z \tag{21}$$

$$F_z = j_\theta \cdot B_r \tag{22}$$

where

$$j_\theta = j_{\theta L} \cdot \cos(\omega_L t + \theta_{j_{\theta L}}) + j_{\theta H} \cdot \cos(\omega_H t + \theta_{j_{\theta H}}) \tag{23}$$

$$B_r = B_{rL} \cdot \cos(\omega_L t + \theta_{BrL}) + B_{rH} \cdot \cos(\omega_H t + \theta_{BrH}) \tag{24}$$

$$B_z = B_{zL} \cdot \cos(\omega_L t + \theta_{BzL}) + B_{zH} \cdot \cos(\omega_H t + \theta_{BzH}). \tag{25}$$

Here, θL and θH represent low and high frequency components of the induced current density j_θ and rL,rH, zL, and zH define r and z components of magnetic induction **B** for low and high frequency components, respectively. By solving these equations, it is simple to show that the superposition of the two frequencies ω_L and ω_H produces alternating force components with the frequencies of $\omega_L + \omega_H$, $\omega_L - \omega_H$ as well as $2\omega_L$, $2\omega_H$ in the liquid metal. Therefore, it would be possible to generate pulsating pressures in the liquid metal having different frequencies and amplitudes. For example, there are alternating force components of 12, 54, 66, 120 Hz, etc., as well as two static components of 6 and 60 Hz when 60 and 6 Hz of current are used as shown in Table 2. It can be seen in this table that there exist two very strong alternating force components (F_r) at 54 and 66 Hz. However, the force components at 120 Hz, even with its high amplitude, will not be effective, as the liquid metal flow cannot respond to such a high frequency alternating force. These strong alternating forces would produce local pulsating flows in the liquid metal and they are believed to be responsible for the increase in k^* value although the overall flow velocity level was decreased as mentioned before.

Sometimes, it may also be useful to adopt a periodic mixing mode (the reversal of the overall vortex flow direction periodically for both single and multifrequency cases) for some specific applications where it is desirable to control the heat transfer process without causing excessive flows, particularly on the melt free surface, which may lead to difficulties, for example, in the melt level control. For this, the optimum time constant has to be selected for each specific application.

In the real DC casting processes, there will be interactions between the overall vortex flow formed by the inductor and the stream of the melt introduced into the casting mold through the spout and float system. Of course, the actual detailed flow patterns and velocity distributions resulted from this interaction will be determined by the direction of the travelling magnetic field and construction of the spout and float system. In addition, the real geometry of the sump (the contour of the liquid/solid interface) will not be spherical, though the radius to depth ratio is likely to be near 1. However,

Table 2
Force components and their amplitudes at 7 A each for 6+60 Hz

Frequency (Hz)		F_r ($\times 10^3$ N/m^3)	F_z ($\times 10^3$ N/m^3)
6		−0.039	−0.286
60		−1.04	−2.74
12	$\cos 2\omega_L t$	0.84	−0.168
	$\sin 2\omega_L t$	−0.43	−0.239
120	$\cos 2\omega_H t$	2.49	2.45
	$\sin 2\omega_H t$	3.72	−1.29
54	$\cos 2(\omega_H - \omega_L)t$	3.51	−1.35
	$\sin 2(\omega_H - \omega_L)t$	3.51	−1.90
66	$\cos 2(\omega_H + \omega_L)t$	6.55	0.51
	$\sin 2(\omega_H + \omega_L)t$	2.27	−2.30

the overall flow patterns in the real DC casting processes is believed to be similar to the toroidal vortex observed in our physical model system, as long as the direction of the travelling magnetic field is downward, which will help to intensify the flow velocity and subsequently the heat transfer at the liquid/solid interface as well as in the bulk without risking producing unnecessary surface perturbations which may cause various surface defects in the cast billets.

6. Conclusions

A special electromagnetic stirrer which can generate an overall vortex flow and local pulsating flow simultaneously has been devised and experimentally tested using a physical model system to evaluate its flow control characteristics and mixing efficiency. The influences of the frequency and current on the flow structure and heat transfer in the liquid In–Ga–Sn eutectic alloy pool were investigated. It has been found that the multifrequency mode, for example $6+60$ Hz, produces more effective heat transfer than the single frequency mode of 60 Hz at the same nominal current level. Moreover, the multifrequency mode consumes about a half of the input energy to the inductor compared to the single frequency mode without causing a significant decrease in the velocity of overall vortex flow. By adopting a simplified non-dimensional mathematical model together with the experimental data, it was possible to predict the velocity level in a given DC casting process and to propose an optimum frequency for the inductor suitable for that specific case. Once the frequencies and amplitude ratio of the multifrequency mode are optimized for a specific application, the design parameters of the inductor can be determined.

References

[1] F. Durand, Convective effects on solidification grain structure, in: S.H. Davis (Ed.), Interactive Dynamics of Convection and Solidification, NATO ASI Series, Kluwer Academic Publishers, Dordrecht, 1992, pp. 81–91.
[2] G.S. Cole, W.C. Winegard, Thermal convection during horizontal solidification of pure metals and alloys, J. Inst. Metals 9 (1964) 153–164.
[3] G.S. Cole, G.F. Bolling, The importance of natural convection in casting, Trans. Met. Soc. AIME 233 (1965) 1568–1572.
[4] D.R. Uhlmann, T.P. Seward, III, B. Chalmers, The effect of magnetic fields on the structure of metal alloy castings, Trans. Met. Soc. AIME 236 (1966) 527–531.
[5] G.S. Cole, G.F. Bolling, Augmented natural convection and equiaxed grain structure in casting, Trans. Met. Soc. AIME 236 (1966) 1366–1368.
[6] V. Kondic, Macrostructure of cast metal, Acta Metallurgica 6 (1958) 660.
[7] F.A. Crossley, R.D. Fisher, A.G. Metcalfe, Viscous shear as an agent for grain refinement in cast metals, Trans. Met. Soc. AIME 221 (1961) 419–420.
[8] F.C. Langenberg, G. Pestel, C.R. Honeycutt, Grain refinement of steel ingots by solidification in a moving electromagnetic field, Trans. Met. Soc. AIME 221 (1961) 993–1001.
[9] W.C. Johnston, G.R. Kotler, W.A. Tiller, The influence of electromagnetic stirring on the nucleation of tin and tin–lead alloys, Trans. Met. Soc. AIME 227 (1963) 890–896.
[10] W.C. Johnston, G.R. Kotler, S. O'Hara, H.V. Ashcom, W.A. Tiller, Grain refinement via electromagnetic stirring during solidification, Trans. Met. Soc. AIME 233 (1965) 1856–1860.
[11] W. Poppmerier, B. Tarmann, O. Schaaber, Application of alternating electromagnetic fields in the continuous casting of steel, J. Met. (1966) 1109–1114.
[12] S. Wojciechowski, B. Chalmers, The influence of mechanical stirring on the columnar to equiaxed transition in aluminium-copper alloys, Trans. Met. Soc. AIME 242 (1968) 690–698.
[13] C. Vives, C. Perry, Effects of electromagnetic stirring during the controlled solidification of tin, Int. J. Heat Mass Transfer 29 (1986) 21–33.
[14] C. Vives, C. Perry, Effects of magnetically damped convection during the controlled solidification of metals and alloys, Int. J. Heat Mass Transfer 30 (1987) 479–496.
[15] P. Desnain, F. Durand, Y. Fautrelle, D. Bloch, J.L. Meyer, J.P. Riquet, Light Metals (1988) 487–493.
[16] C. Vives, Effects of forced electromagnetic vibrations during the solidification of aluminium alloys: Part II. Solidification in the presence of colinear variable and stational magnetic fields, Metall. Trans. B27 (1996) 457–464.
[17] H.S. Marr, Electromagnetic stirring: stepping stone to improved continuously cast products, Iron and Steel Int. (1979) 29–41.
[18] K. Buxmann, Electromagnetic DC casting of aluminium (EMC)-Status and new perspectives, Science and Engineering of Light Metals (1991) 1015–1022.
[19] K.H. Spitzer, G. Reiter, K. Schwerdtfeger, Volume force design in liquid metals by multifrequency electromagnetic stirring, Proceedings of the International Symposium on Electromagnetic Processing of Materials, Iron and Steel Institute of Japan, 1994, pp. 178–183.
[20] R. Ricou, C. Vives, Local velocity and mass transfer measurements in molten metals using an incorporated magnet probe, Int. J. Heat Mass Transfer 25 (1982) 1579–1588.
[21] C. Vives, R. Ricou, Experimental study of continuous electromagnetic casting of aluminium alloys, Metal Trans. B16 (1985) 377–384.
[22] J.M. Gelfgat, O.A. Lielausis, E.V. Shcherbinin, Liquid Metal under the Action of Electromagnetic Forces, Zinatne, Riga, 1976, p. 13.
[23] S.H. Chung, Y.W. Cho, J.D. Shim, J. Korean Inst. Metals Mater. 36 (1998) 924–935.